# REPORT DOCUMENTATION PAGE

AFRL-SR-AR-TR-05-

0222



| 1. AGENCY USE ONLY *(Leave blank)* | 2. REPORT DATE | 3. REPORT TYPE AND DATES COVERED |
|---|---|---|
| | | 15 JAN 2004 - 14 OCT 2004 FINAL |

**4. TITLE AND SUBTITLE**
DEVELOPMENT OF III-V TERAHERTZ QUANTUM CASCADE LASERS

**5. FUNDING NUMBERS**
65502F
STTR/TX

**6. AUTHOR(S)**
DR DABIRAN

**7. PERFORMING ORGANIZATION NAME(S) AND ADDRESS(ES)**
SVT ASSOCIATES INCORP
7620 EXECUTIVE DRIVE
EDEN PRAIRIE MN 55344-3677

**8. PERFORMING ORGANIZATION REPORT NUMBER**

**9. SPONSORING/MONITORING AGENCY NAME(S) AND ADDRESS(ES)**
AFOSR/NE
4015 WILSON BLVD
SUITE 713
ARLINGTON VA 22203

**10. SPONSORING/MONITORING AGENCY REPORT NUMBER**
FA9550-04-C-0027

**11. SUPPLEMENTARY NOTES**

**12a. DISTRIBUTION AVAILABILITY STATEMENT**
DISTRIBUTION STATEMENT A: Unlimited

**12b. DISTRIBUTION CODE**

**13. ABSTRACT** *(Maximum 200 words)*

A very successful Phase I project on semiconductor THz laser has been carried out. Several innovative techniques have been demonstrated during the performance of this work. The most significant concept being a different approach to how the laser should be pumped, resulting in more efficient THz output generation. We called this concept Separate Electrical and Waveguiding (SEW) structure that circumvents the radiation absorption in the doped waveguide region in a conventional THz device, leading to lower threshold and higher temperature operation. In addition we have developed an electrical measurement to detect lasing threshold, and a packaging technique for solid, effective thermal contact during measurement.

| 14. SUBJECT TERMS | 15. NUMBER OF PAGES |
|---|---|
| | 16. PRICE CODE |

| 17. SECURITY CLASSIFICATION OF REPORT | 18. SECURITY CLASSIFICATION OF THIS PAGE | 19. SECURITY CLASSIFICATION OF ABSTRACT | 20. LIMITATION OF ABSTRACT |
|---|---|---|---|
| Unclassified | Unclassified | Unclassified | UL |



6-14-05

ORIGINAL

# Development of III-V Terahertz Quantum Cascade Lasers

STTR Phase I Research and Development Program

## Final Report

Contract #FA9550-04-C-0027

February 14, 2005
Total Contract Value $99,969.00

*Submitted to:*

Dr. Gernot Pomrenke
Air Force Office of Scientific Research
Ballston Common Towers III
4015 Wilson Blvd. Room 713
Arlington VA 22203-1954
Phone: 703-696-8426
gernot.pomrenke@afosr.af.mil

*Submitted by:*

Dr. Sergey Zaytsev
SVT Associates
7620 Executive Drive
Eden Prairie, MN 55344
Phone: (952) 934-2100 x247
Fax: (952) 934-2737
zaytsev@svta.com

The Contractor, SVT Associates, hereby declares that, to the best of its knowledge and belief, the technical data delivered herewith under Contract No. DASG60-02-P-0129 is complete, accurate, and complies with all requirements of the contract.

Date_____

Name and Title of Authorized Official _____



ORIGINAL

## Table of Contents

## Executive Summary

A very successful Phase I project on semiconductor THz laser has been carried out. Several innovative techniques have been demonstrated during the performance of this work. The most significant concept being a different approach to how the laser should be pumped, resulting in more efficient THz output generation. We called this concept Separate Electrical and Waveguiding (SEW) structure that circumvents the radiation absorption in the doped waveguide region in a conventional THz device, leading to lower threshold and higher temperature operation. In addition we have developed an electrical measurement to detect lasing threshold, and a packaging technique for solid, effective thermal contact during measurement.

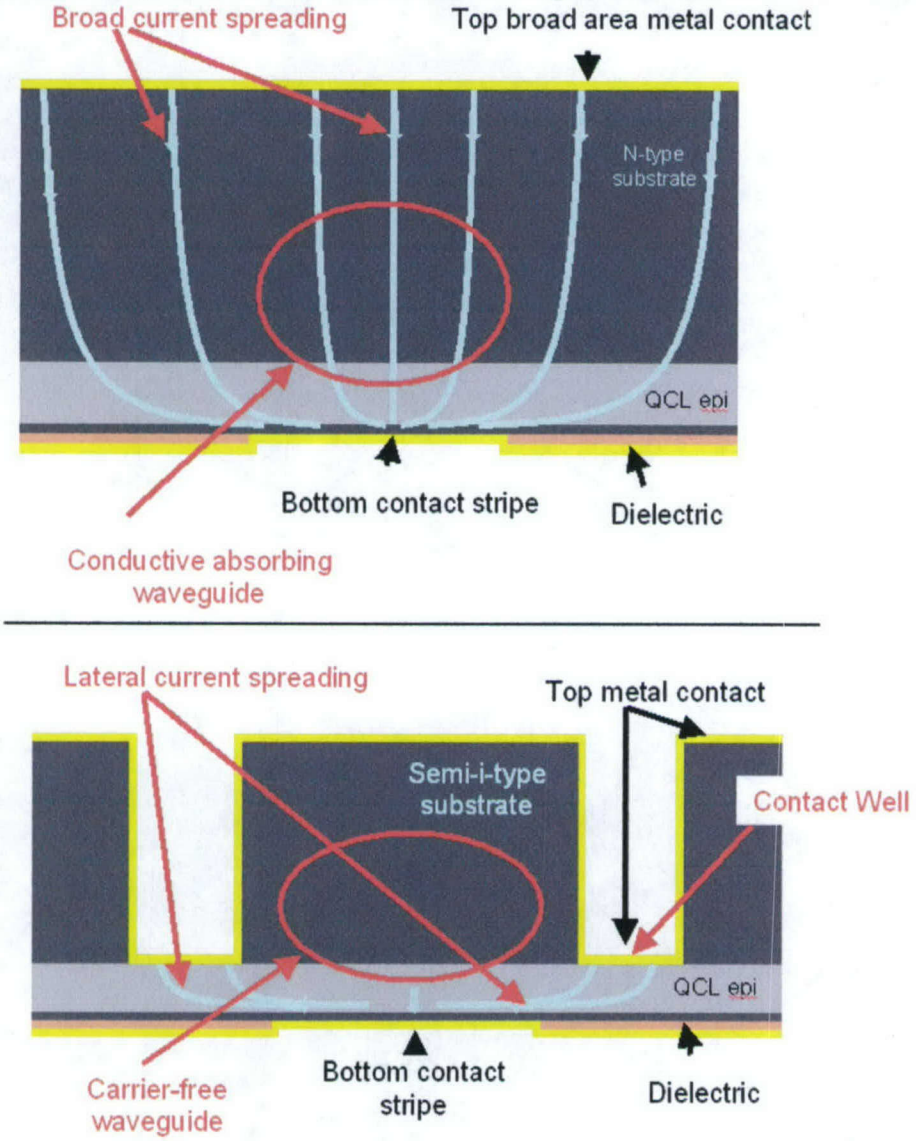


**Figure 1. Separate Electrical & Waveguiding (SEW) structure of the new concept (lower figure) compared with a conventional THz laser structure (upper).**

The improvement achievable with the SEW concept may be described as follows. Due to the very long wavelength of the THz radiation, the waveguide required is too thick to be formed from epitaxial material, and instead by thinning down the substrate to appropriate thickness. On the other hand, in order to provide the electrical contact from the substrate side the wafer itself is heavily doped. This structure is shown schematically upside down in the upper figure in Figure 1. The epi-side of the contact is through a deposited conducting layer and metallization. The high dopant concentration in the waveguide leads to high optical loss caused by free carrier absorption, which in turn results in significant increase in threshold current. In addition the thickness of the wafer increases contact resistance and broad current spreading.

The SEW concept by contrast utilizes un-doped substrate for laser structure growth. As shown in the lower figure in Figure 1, holes are cut through the thickness of the substrate to an etch-stop layer before metallization is deposited. As a result, very low absorption occurs in the carrier free waveguide region.

This device concept was applied to both a conventional THz QCL structure, and to a new Closed-Coupled Quantum Well structure proposed by Prof. Ray Tsu of University of North Carolina at Charlott, our university partner on the program. Key accomplishments of the project are summarized below

***-Developed and fabricated SEW THz structure***

***-Demonstrated near Liquid Nitrogen temperature operation***

***-Shown low lasing threshold***

***-Refined IdV/dI electrical characterization method***

***-Conceived and tested the novel Close-coupled QW structure***

## THz Laser Structure Design

The goal of this Phase I program is the demonstration of a Quantum Cascade Laser (QCL) for operation in the THz frequency regime within the window of the Optical-Acoustical phonons, i.e., ~ 35meV. Our design was, in part, motivated by the one introduced by F. Capasso et al. IEEE J. Q. Electronics 33 89 1997, for a QCL operating at $\lambda$=9.3 $\mu m$. Their design utilized transitions between the n=3 to n=2 energy levels of a quantum well (emitter) and a superlattice (SL) (collector-emitter). The transition to level 2 is aligned with the miniband of the SL which, in turn, is aligned with level 3 of the active QW in the next period. For THz operation at 34.5meV (i.e., $\lambda = 36\ \mu m$), however, QWs are required whose lowest energy level is at least $k_BT$ = 25meV at room temperature. Moreover, the highest energy level must be sufficiently below the top of the barrier level in order to prevent tunneling by the injected electrons except through resonance. Fig 1(a) shows the band structure without an applied voltage while Fig 1(b) shows the band structure for an applied voltage corresponding to an electric field of ~ $2 \cdot 10^4$ V/cm. For the latter, the energy levels are matched to allow resonant tunneling for injection and collection after an optical transition with emission of THz radiation takes place.
Based on these considerations, we designed a QCL to meet the following requirements:

(1) The active region consists of $A_1$, an upper level to receive the injected electrons, making a transition to $A_2$, a lower level to receive the electrons after emission of a photon at 35meV, to be collected by the SL collector-emitter. The separation $A_1$- $A_2$ = 35meV at the operating voltage V, determined by injection via resonant tunneling from the emitter.
(2) Since $A_1$ is sufficiently below the top of the barrier, and there is no state at the receiving end, the injected electron at $A_1$ can only make a downward transition and be collected.
(3) Essentially our design introduces a thin barrier between the two sections of the quantum well to form a higher state (symmetric state) and a lower state (anti-symmetric state). The width w of the well and the thickness of the barrier can be adjusted at the operating voltage V.
(4) The emitter is chirped to take the electrons from the n+ contact, for $2 \times 10^{18}$ $cm^{-3}$, (a relatively low doping compared to Capasso et al.) to preserve good mobility, and shifted to match the position of the upper level $A_1$.
(5) On the receiving side, we have a chirped SL to take the electrons at $A_2$ and shifted up to match the state $A_1$ of the next QCL period.

In Fig 1, basic elements of the heterostructure design are the following:

1. $C_1$ and $C_2$ are the right and left contacts.
2. $Q_i$ are chirped QWs to be aligned under an applied voltage to the Fermi level at the left contact.

3. Electrons are injected into the state $A_1$ of the active regions. Following an A.P interaction, where A is the vector potential of the photons, electrons make transitions to the lower energy level $A_2$.
4. $A_2$ must be aligned with SL-band, shown as a chirped SL.
5. The photon energy is determined by the coupling of the two QWs in the active regions, which can be adjusted by changing the width of the barrier. Without coupling, $A_1$ and $A_2$ are equal. The applied voltage negligibly affects the separation because in RTD these states are tied to the bottom of the voltage, moving up and down together.
6. Electrons exiting from $A_2$ are at a much higher energy then $C_2$. Therefore, we use a SL coupled QWs designed with a chirp to allow the energy of electrons entering at the left to be lowered to a value near the level of $C_2$ so that the momentum loss is not all converted to heat all at the right contact.
7. The emitter is chirped to align the Fermi level at the contact to $A_1$ in the active region. The multiple barriers in the chirped SL should be thin, leading to a broad band to facilitate the ability of collected electrons to travel to the right contact. The photon energy is again determined by the coupling of the two QWs in the active regions.

To illustrate the process, consider a QCL operating at 10THz. Then $\lambda$=30μm, which corresponds to 0,042eV or, equivalently, 42meV. For GaAs and a well width of 5nm, the required energy level is 0.08eV. To attain an energy level splitting of 0.04eV, a barrier ~ 1nm is required. In other words, the right and left QWs in the active region must be 5nm in width and separated by a 1nm barrier. For a doping level of $2x10^{18}$ $cm^{-3}$, $E_F$ = 80meV. The first well should have a width of 4nm and an energy state ~ 0.1eV slightly above $E_f$, which can be aligned with $E_F$ by an applied voltage. It will be necessary to align $Q_1$ with $A_1$. At V=0 $A_1$ is 0.08+(0.04/2) = 0.1eV. Then, depending on the number of chirped QW emitter layers, we can calculate the voltage at points within the active region since we know the well widths for $Q_2$, $Q_3$, etc. The barrier widths can be assumed fixed at 2nm in the emitter to allow broadening of the levels to achieve easy alignment with $A_a$. The same procedure can be used on the collector side. Chirping on the collector allows the energy level to be lowered to near $E_f$ at the collector contact.

The main restriction is to operate outside the phonon regions: LO-TO is between 50-44 meV and LA-TA is between 36-34 meV. This leaves a window between 36 and 44 meV, i.e., $\lambda = 34 - 28\mu m$.

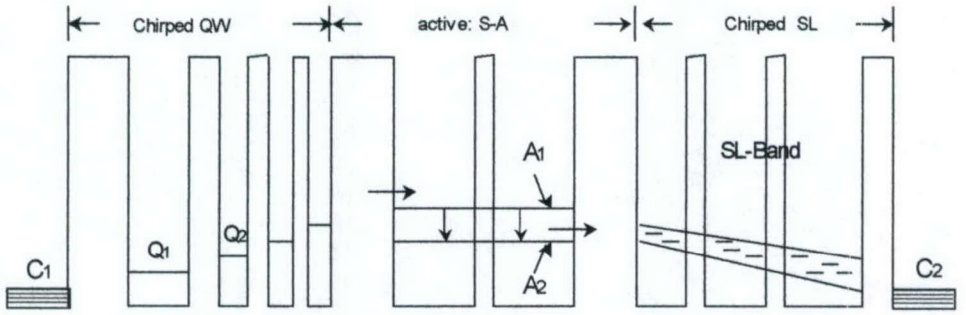


a)

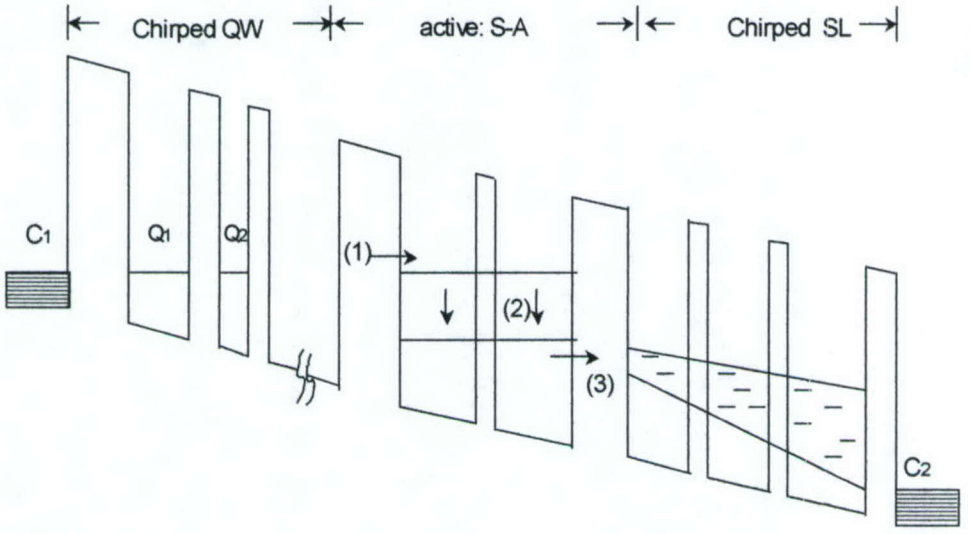


b)

Fig. 1. Principle of the bandgap structure of the proposed THz QC lasers based on coupled quantum wells: a – unbiased structure, b- bias with an electric field of $2 \cdot 10^4$ V/cm$^2$.

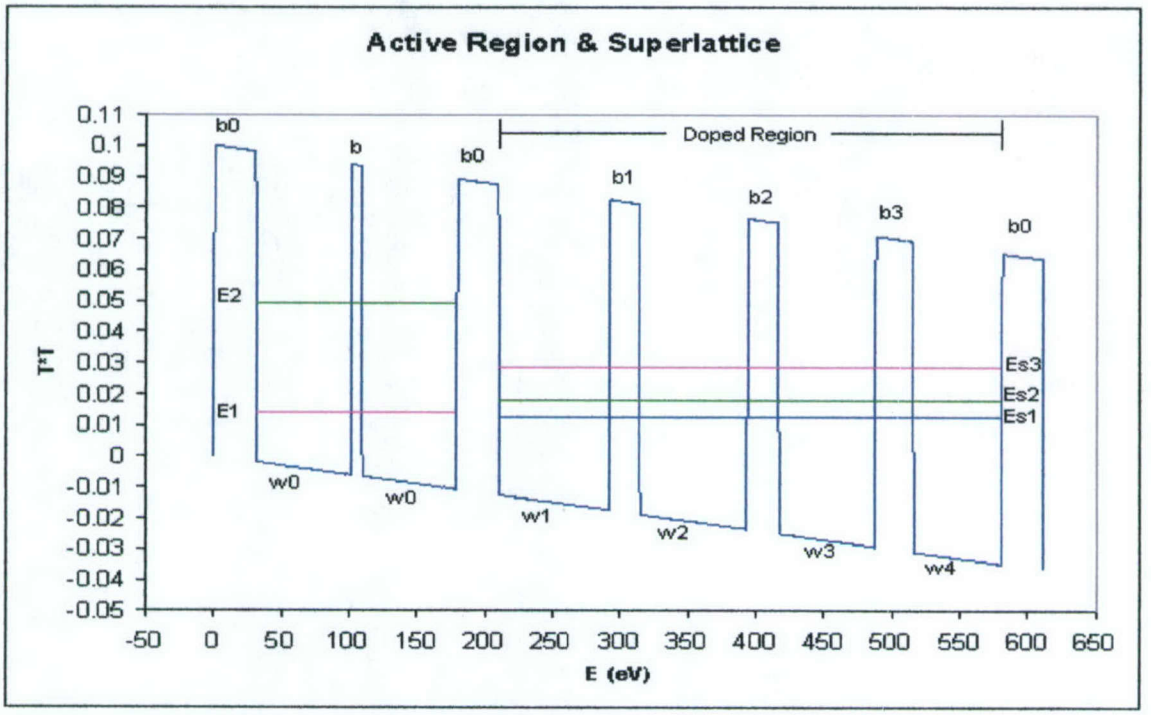


Fig. 2. Final structure of THz QCL with applied direct bias.

In Fig 2, basic elements of the heterostructure design are following:

**$Al_{0.15}Ga_{0.85}As/GaAs$ Structure (Å):**
Active Region: **b0**/w0/**b**/w0/**b0=31**/70/ **8**/70/**31**
Superlattice Injector: **b0**/w1/**b1**/w2/**b2**/w3/**b3**/w4/**b0=31**/82/**22**/79/**23**/71/**28**/65/**31**
**Design Parameters:**
Mass: $m_w=0.067m_0$, $m_b=0.0689m_0$
$\Delta E_c=0.1$ eV
**Active Region: (F=6 KV/cm)**
E2=0.0490 eV
E1=0.0142 eV
ΔE=0.0348 eV
**Superlattice: (F=6 KV/cm)**
Es3=0.0286 eV
Es2=0.0179 eV
Es1=0.0125 eV

**Reference**: Carlo Sirtori, et al, IEEE Journal of Quantum Electronics, V33, No.1, Page 89 Jan 1997

Final design of Quantum Cascade Laser for operation in THz range converted into technological format for MBE growth is as following:

**Layer Structure Specification**

| Product: | QCL R.T. design (SVTA proprietary) |
|---|---|

| Layer | Material | Group | Repeat | Mole fraction (x) | | Thickness | Doping profile | | Type | Dopant |
|---|---|---|---|---|---|---|---|---|---|---|
| | | | | start | finish | (A) | start | finish | | |
| 20 | GaAs | | | | | 800 | 5e18 | | N | Si |
| 19 | | 1 | 25 | | | 65 | 2e17 | | N | Si |
| 18 | Al(x)Ga(1-x)As | 1 | 25 | 0.15 | | 28 | 2e17 | | N | Si |
| 17 | | 1 | 25 | | | 71 | 2e17 | | N | Si |
| 16 | Al(x)Ga(1-x)As | 1 | 25 | 0.15 | | 23 | 2e17 | | N | Si |
| 15 | | 1 | 25 | | | 79 | 2e17 | | N | Si |
| 14 | Al(x)Ga(1-x)As | 1 | 25 | 0.15 | | 22 | 2e17 | | N | Si |
| 13 | | 1 | 25 | | | 82 | 2e17 | | N | Si |
| 12 | Al(x)Ga(1-x)As | 1 | 25 | 0.15 | | 31 | | | u.d. | |
| 11 | | 1 | 25 | | | 70 | | | u.d. | |
| 10 | Al(x)Ga(1-x)As | 1 | 25 | 0.15 | | 8 | | | u.d. | |
| 9 | | 1 | 25 | | | 70 | | | u.d. | |
| 8 | Al(x)Ga(1-x)As | 1 | 25 | 0.15 | | 31 | | | u.d. | |
| 7 | | | | | | 65 | 2e17 | | N | Si |
| 6 | Al(x)Ga(1-x)As | | | 0.15 | | 28 | 2e17 | | N | Si |
| 5 | | | | | | 71 | 2e17 | | N | Si |
| 4 | Al(x)Ga(1-x)As | | | 0.15 | | 23 | 2e17 | | N | Si |
| 3 | | | | | | 79 | 2e17 | | N | Si |
| 2 | Al(x)Ga(1-x)As | | | 0.15 | | 22 | 2e17 | | N | Si |
| 1 | | | | | | 82 | 2e17 | | N | Si |
| 0 | Al(x)Ga(1-x)As | | | 0.15 | | 31 | 2e17 | | N | Si |
| 1 | GaAs | | | | | 1000 | 5e18 | | N | Si |
| | Al0.3Ga07As | | | 0.3 | | 3000 | 5e18 | | | |
| | GaAs | Buffer | | | | 1000 | 5e18 | | | |
| 0 | Substrate | U.D. | | | | | | | | |

Table 1. THz QC laser structure for 30 μm wavelength designed at University of North Carolina for present project.

In parallel, for fabricating and testing the SEW concept, a "classical" THz QCL wafer has been grown, similar to one reported by M. Rochat at al, (APL v.81, 8, pp.1382-1383). However, since we planned different laser stripe design and packaging, the wafer has been grown on undoped substrate, to reduce optical losses caused by free carrier absorption. Structure of this wafer is listed in Table 2.

**Layer Structure Specification**

| Product: | Classical QCL |
|---|---|

| Layer | Material | Group | Repeat | Mole fraction (x) | | Thickness | Doping profile | | Type | Dopant |
|---|---|---|---|---|---|---|---|---|---|---|
| | | | | start | finish | (nm) | start | finish | | |
| 20 | GaAs | | | | | 80 | 5e18 | | N | Si |
| 19 | Al(x)Ga(1-x)As | | | 0.15 | | 10 | | | u.d. | |
| 18 | Al(x)Ga(1-x)As * | | | 0.15 | 0 | 320 | | | u.d. | |
| 17 | Al(x)Ga(1-x)As | 1 | 120 | 0.15 | | 3 | | | u.d. | |
| 16 | | 1 | 120 | | | 18.6 | | | u.d. | |
| 15 | Al(x)Ga(1-x)As | 1 | 120 | 0.15 | | 0.7 | | | u.d. | |
| 14 | | 1 | 120 | | | 15.4 | | | u.d. | |
| 13 | Al(x)Ga(1-x)As | 1 | 120 | 0.15 | | 0.5 | | | u.d. | |
| 12 | | 1 | 120 | | | 13.6 | | | u.d. | |
| 11 | Al(x)Ga(1-x)As | 1 | 120 | 0.15 | | 2.3 | | | u.d. | |
| 10 | | 1 | 120 | | | 12.8 | | | u.d. | |
| 9 | Al(x)Ga(1-x)As | 1 | 120 | 0.15 | | 1.8 | | | u.d. | |
| 8 | | 1 | 120 | | | 11.8 | 1.6e16 | | N | Si |
| 7 | Al(x)Ga(1-x)As | 1 | 120 | 0.15 | | 2.3 | 1.6e16 | | N | Si |
| 6 | | 1 | 120 | | | 10.8 | 1.6e16 | | N | Si |
| 5 | Al(x)Ga(1-x)As | 1 | 120 | 0.15 | | 3.2 | | | u.d. | |
| 4 | | 1 | 120 | | | 10.4 | | | u.d. | |
| 3 | Al(x)Ga(1-x)As * | | | 0 | 0.15 | 320 | | | u.d | |
| 2 | Al(x)Ga(1-x)As | | | 0.15 | | 15 | | | u.d | |
| 1 | GaAs | | | | | 300 | 2e18 | | N | Si |
| 0 | Substrate | U.D. | | | | | | | | |

Table 2. THz QC laser structure reported by M. Rochat at al, (APL v.81, 8, pp.1382-1383) used in present work as for SEW testing.

## Growth Calibration and Wafer Growth

### Temperature control in MBE growth.

MBE inherently has a great degree of flux control, so the layer thicknesses are readily determined by the amount of time the source cell shutters are open. Substrate temperature control, however, can be a more difficult challenge. To cope with this issue, we have recently employed a pyrometer/interferometer designed and built by SVTA. It is marketed under the name "In-Situ 4000 Process Monitor" and provides two-color pyrometry and two channels of narrowband reflectometry in a single instrument. This instrument is designed to correct many of the problems encountered in traditional pyrometry during MBE such as:

- Substrate transparency
- Window coating.
- Multilayer interference effects
- Changing and unknown substrate emissivity.

The problem of time varying or unknown emissivity is addressed by the addition to the pyrometry of specular reflectometry at the same wavelength at the 950 nm pyrometry. If the substrate is opaque and the front surface of the substrate remains smooth, then the emissivity, $\varepsilon$, of the substrate/film system may be calculated via $\varepsilon=1-R$ where R is the reflectance at the same wavelength. Thus, as the substrate emissivity changes, and the multilayer optical interference of film deposited on the surface affects the transmission of radiation to the pyrometer, the In-Situ 4000 is able to compute the correct emissivity and provide an accurate temperature measurement during thin film growth. An additional channel of reflectometry at 470 nm is provided to measure film thickness and index of refraction during growth. The system was designed and is manufactured entirely by SVT Associates, with the end result being improved control in the substrate temperature during growth. The system includes a communications interface to a personal computer where an SVTA designed software application performs temperature and thickness calculations in real time (Fig. 2).

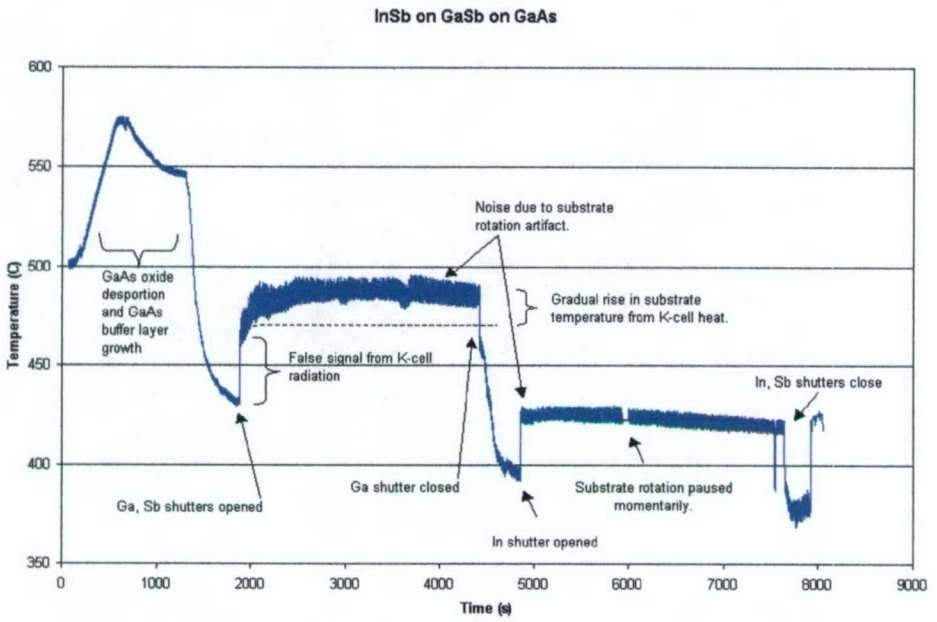


**Figure 3**. Substrate temperature data from the SVTA IS4K interferometer/pyrometer during the growth of GaSb and InAs on a GaAs wafer.

**Procedure of growth rates calibration for Quantum Cascade Laser structure**

For growth process calibration, and for verification of interface quality, special runs with reduced number of periods have been performed. Corresponding samples have been studied using both by X-ray methods and photoluminescence, to prove material quality. Fig. 1a shows rocking curve and numerical simulation for calibration wafer with following structure:

| | | | |
|---|---|---|---|
| | GaAs | substrate | N+ |
| | GaAs | 300nm | |
| 50 times | $Al_{0.15}GaAs$ | 2.3nm | |
| 50 times | GaAs | 12.8nm | |

The curve indicates good crystalline quality, acceptable for the quantum cascade laser.

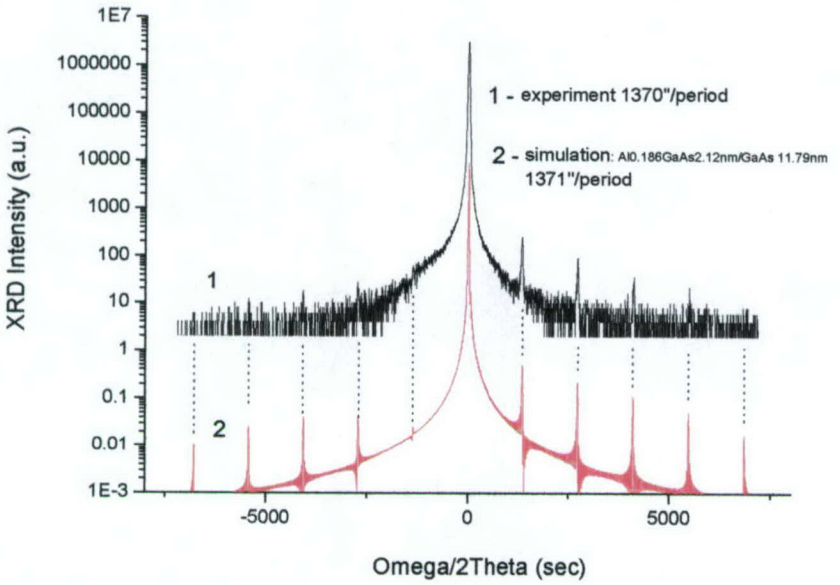


Fig. 4. Results of X-ray analysis of the calibration wafer. SL period thickness is found to be 13.85 nm.

Automatic structure simulation by direct analysis is hardly possible since very low average Al composition leads to low value of signal and high noise influence. However, period of SL can be easily found.
Given period of the SL (13.8 nm) and assuming the same growth rate of GaAs we can estimate the growth rate of AlAs:

Parameters of DO-306 expected and extracted from XRD measurements

| Parameter | Expected value | Obtained value |
|---|---|---|
| *Extracted from the experiment* | | |
| SL period | 15.1 nm | 13.85 nm |
| *Recalculated assuming GaAs growth rate the same as in the case of bulk AlGaAs* (2.73 A/sec) | | |
| AlGaAs layer thickness | 2.3 nm | 2.54 nm |
| GaAs layer thickness | 12.8 nm | 11.31 nm |
| AlAs growth rate | 0.53 A/sec | 0.63 A/sec |
| GaAs growth rate | 3 A/sec | 2.73 A/sec |
| AlGaAs growth rate | 3.53 A/sec | 3.36 A/sec |
| Al content in AlGaAs | 15% | 18.8% |

Photoluminescence of specially grown wafers has been measured to check exact composition of the AlGaAs layers. The wafer structure was following:

| | | |
|---|---|---|
| GaAs | substrate | s.i. |
| GaAs | 300nm | |
| $Al_{0.15}GaAs$ | 200nm | |
| $Al_{0.15}GaAs$ | 900nm | :Si 1.6e16cm-3 |
| GaAs | 5nm | :Si 1.6e16cm-3 |

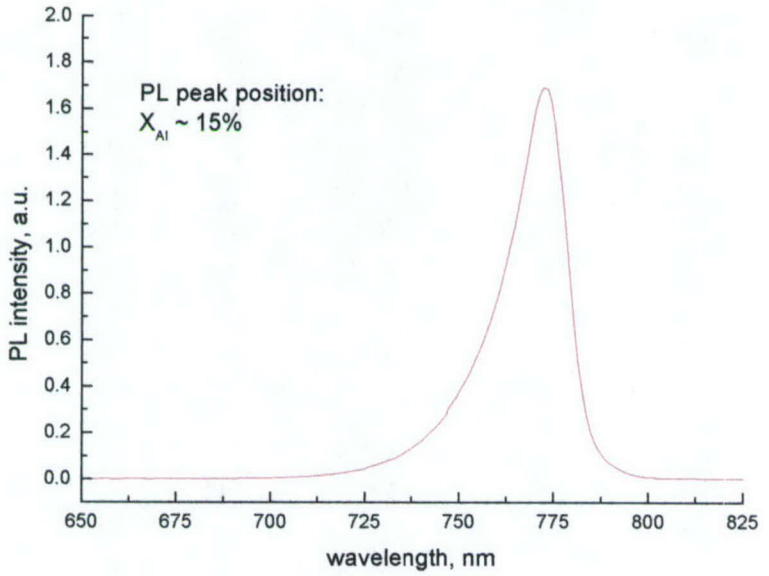


Fig. 5. Photoluminescence spectrum of $Al_{0.15}Ga_{0.85}As$ layer

Assuming 12.5 nm blue shift of PL peak position per one percent of Al in AlGaAs the aluminum content can be estimated by the following equation:

$$x = (1240/\lambda - 1.42)/0.0125 = 14.7\ \%$$

This value is in good agreement with corresponding XRD data and expected value. Special quantum cascade structure developed at University of North Carolina for this project is presented in Table 1. It has been grown after we finished growth of reference structure mentioned above.

To optimize the growth mode and to ensure proper precision, new set of calibration runs of MBE system has been done and corresponding wafers have been tested. Results of these tests are presented below.

For growth process calibration, and for verification of interface quality, special runs with reduced number of periods have been performed. Corresponding samples have been studied using both X-ray methods and photoluminescence, to prove material quality. Fig. 6 and Fig. 7 show rocking curve and numerical simulation for calibration wafer with following structure:

GaAs substrate N+
GaAs 300nm
200 times $Al_{0.3}GaAs$ 1.53nm
200 times GaAs 2.97nm

The curve indicates good crystalline quality, acceptable for the quantum cascade laser.

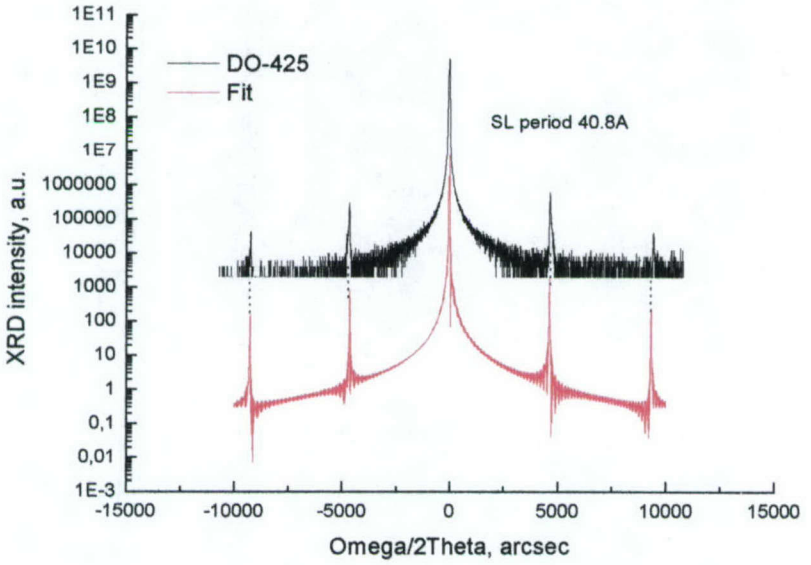


**Fig. 6.** XRD rocking curve from AlGaAs/GaAs superlattice and simulation curve in a wide angle range.

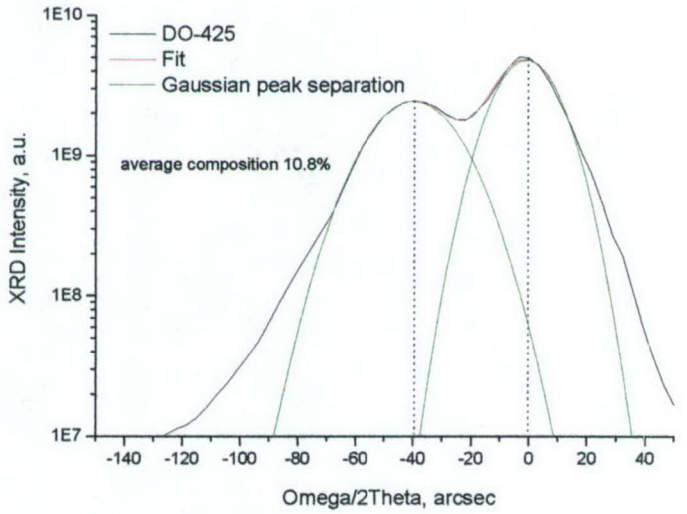


**Fig.7.** XRD rocking curve from AlGaAs/GaAs superlattice and simulation curves in a narrow angle range around the substrate.

**Results of analysis are:**

| | |
|---|---|
| Average Al composition (%): | **10.8** |
| SL Period Thickness (nm): | **4.08** |

Growth of AlGaAs/GaAs QCL implies usage of Al cell for short time. It will result into flux overshot effect as compared with growth of thick layers. In order to identify the correspondence of growth rate calibration it is necessary to grow a calibration sample with short-period superlattice. Since the Ga shutter is open during the whole QCL structure the most crucial thing in the calibration is the shutter effect on Al cell. The test structure is designed in such a way that the durations of the layer depositions and Al growth rate are kept as in the final structure, but the Ga growth rate is adjusted to achieve well resolved XRD spectrum, with peaks attributed to average composition and superlattice period.

**Adjustment of cell temperature for the growth of final structure.**

Cell temperatures necessary for growth of final structure can be extracted based on results obtained and growth rate (flux) dependences on cell temperature. Both RHEED oscillations and post-growth XRD measurements were used to precisely determine the growth rates of Al and Ga.

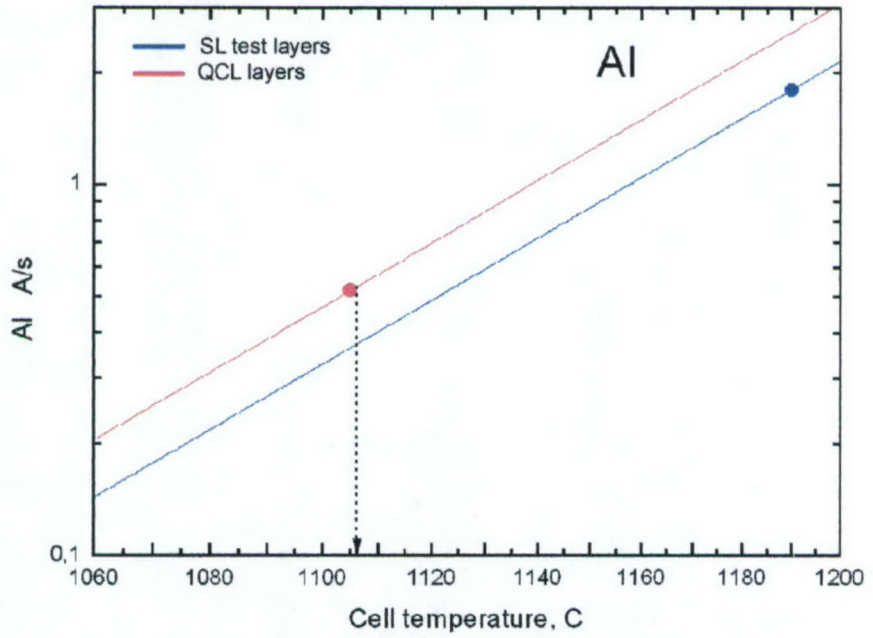


**Fig. 8.** Dependence of GaAs growth rate for Ga cell on the cell temperature.

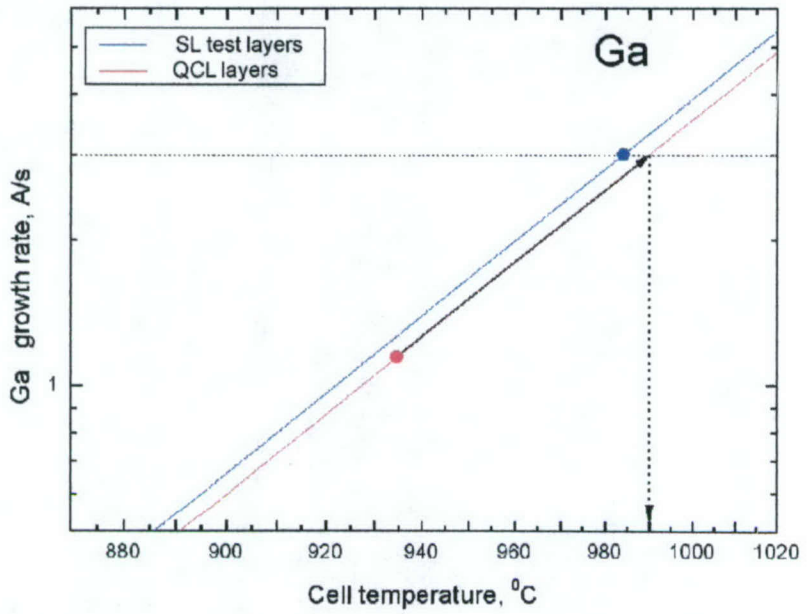


**Fig. 9.** Dependence of AlAs growth rate for Al cell on the cell temperature.

Marked with blue is the data obtained using a AlAs/GaAs superlattice (thick layers > 1000 Å) by optical reflectance measurements. Marked in red is the data obtained from the XRD measurements of the QCL structure, which uses thinner layers (~ 100 Å). Points show real measured values, while lines are temperature dependencies based on corresponding flux measurements.

**Table 3.** Corrected temperatures for Al and Ga cells for QCL structure

| Cell | Ga (°C) | Al (°C) |
|---|---|---|
| Growth temperature for GaAs/AlAs SL | 984 | 1190 |
| Real growth rate, nm/s | 0.300 | 0.180 |
| Growth temperature for QCL structure | 934.6 | 1105 |
| Real growth rate, nm/s | 0.114 | 0.0518 |
| Target growth rate, nm/sec | 0.300 | 0.053 |
| Corrected growth temperature, °C | **990** | **1106,3** |

Slight adjustments were made to the effusion cell temperatures for growing the QCL structure. Thus, temperature of Ga cell of 990°C and temperature of Al cell of 1106.3 °C will **provide exact layer composition and thickness in the final structure**.

Taking into account results of above calibrations, growth of the second QCL wafer has been successfully performed.

**Processing, Mask Design and Packaging**

Due to the very long wavelength of the THz radiation, it is impossible to form a waveguide by epitaxial growth – its thickness should be at least several tens of microns. In existing lasers of this kind the substrate thinned by lapping down to approximately 100 μm is used as a waveguide. However, to provide electrical pumping between top and bottom contacts, this substrate must be doped. It is well known, that doping of the laser waveguide leads to strong optical losses caused by free carrier absorption, and leading to significant increase in threshold current. Such losses also reduce the laser output efficiency and, as a result, shrink temperature range of the laser operation. To reduce such losses, we decided to use undoped substrates. This made it impossible to use the substrate for a bottom contact of the laser.

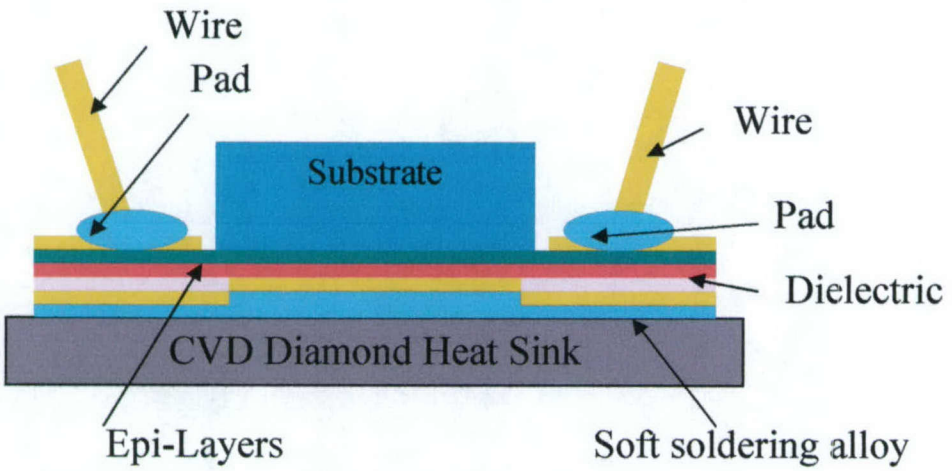


**Fig. 10**. Concept of THz laser design and its packaging.

Typically, such problem is solved by deep mesa etching down to bottom contact layer. However, in our case the corresponding highly doped contact layer lies right on top of the substrate and is buried under multi-layer 15 μm thick QC structure. Selective etching through such structure can be a challenge. That is why we etched a special deep groove through the substrate to provide contact to this layer from the bottom side. Corresponding holes are located on sides of the waveguide, providind "lateral" pumping of the active region. Our estimates demonstrated that with such unusually thick active layer lateral pumping may provide satisfactory uniformity, while thick undoped substrate can form transparent (yet asymmetric) waveguide. Our mask design includes also stripe geometry electrical isolation on the epi side of the wafer, to provide electrical confinement. Our estimates show that given lateral current spreading 100 μm wide stripe should provide conditions for single transverse mode lasing. Our mask design included also 75 μm and 50 μm stripes.

As it was mentioned above, since QCL wafer consists of large number of thin layers with different composition, it is difficult to etch it through and stop precisely in the

bottom contact layer. However, because our heterostructure is grown on undoped semi-insulating substrate, it was impossible to deposit contact metallization directly on the substrate after lapping. As it has been described in previously, we selectively etched deep trenches through the substrate down to the highly doped layer after lapping the wafer. For this purpose we introduced special high aluminum content etch stop layer in our wafer design. Our experiments were focused on the optimization of the selective wet etching procedure. Wet etching is isotropic by nature and it is important to make sure that undercut which takes place during such deep etching remains reasonably low. Fig. 11 illustrates the problem.

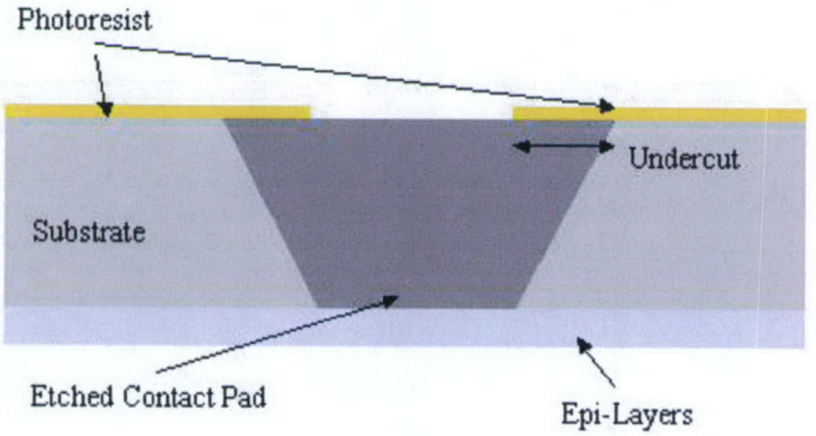


**Fig. 11.** Schematic view of deep contact pad etching (cross section of the wafer).

Fig. 12 - 15 show experimental results. In our mask design, 50 μm hexagon shapes are used for back side contacts. We etched GaAs wafer over 70 μm deep using selective isotropic etchant. Microscope image taken in Nomarski mode indicates that photoresist remains mostly undamaged (apart from its very rim) even after such long etching. Bottom of the formed trench is flat, and undercut is still short enough. Insert in this figure shows a calibration scale.

Selective etchant consisting of 1:20 $NH_4OH:H_2O_2$ has been used for the wells etching. Etch time was a total of 45 min at RT. Unfortunately, variation of the well size and shape was significant, and etching repeatability requires more work in the future. It is important to notice, that the thickness of the epi layers was found to be high enough to provide integrity of the wafer during its cleaving. We have been able to form clean facets to obtain good reflectivity at the laser edges.

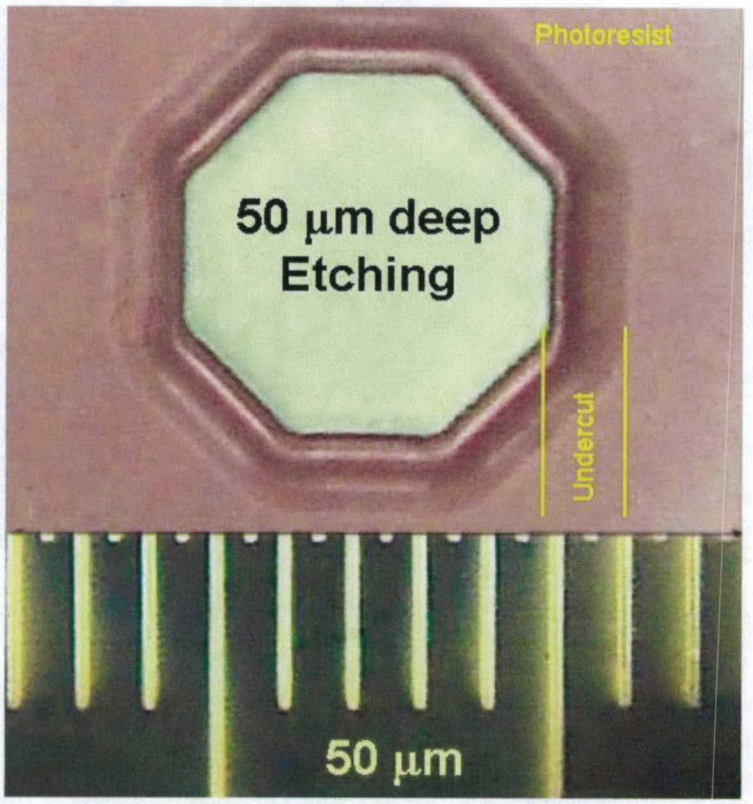


**Fig .12.** Top view of the 50 μm deep contact pad etched with significant undercut.

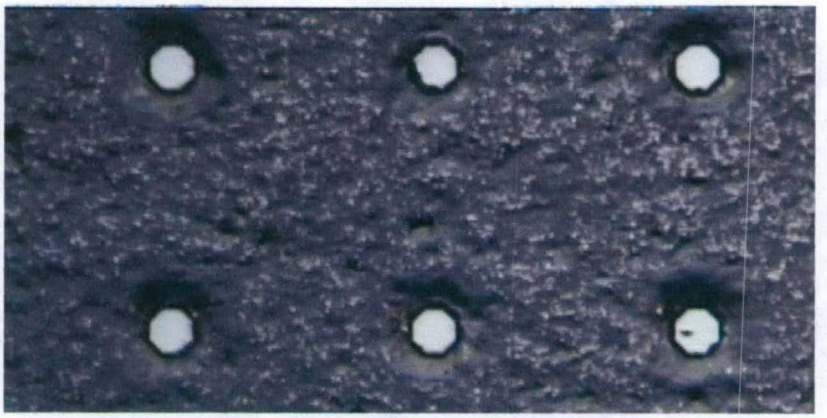

**Fig. 13.** Deep mesa etching on dummy wafer. Etch stop layer provides flat bottom of trenches even when original surface is rough..

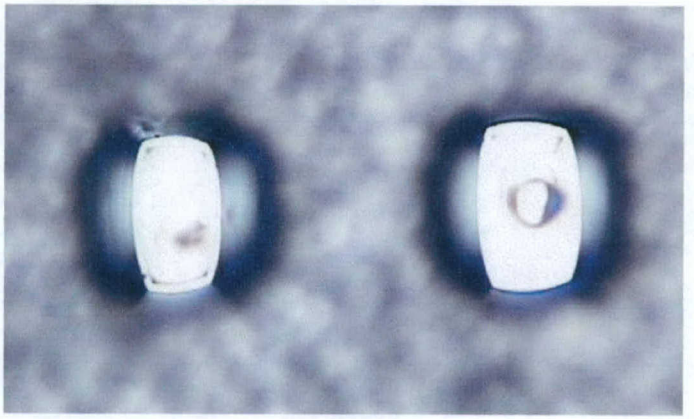

**Fig. 14.** Anisotropy of the wet etching changes shape of the bottom of contact wells from octagons to elongated rectangle.

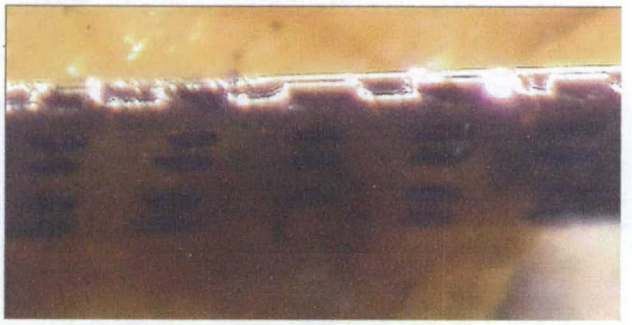

a)

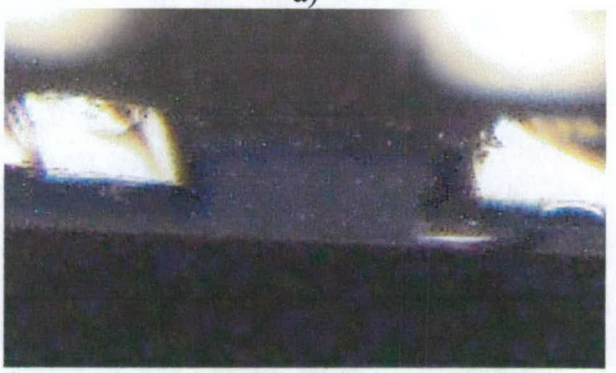

b)

**Fig. 16 a, b.** Cross section of the THz laser wafer with deep contact wells.

**Contact metallization**

Dual technique has been used to create reliable contacts to the laser. First, we performed e-beam deposition of the multi-layer ohmic contact followed by annealing (discussed below), and then we additionally made thin gold plating of the entire back

surface of the wafer to make sure that sidewalls of trenches are completely coated and provide good electrical conductivity.

Another important process optimization needed for normal operation of THz QCL is providing of low contact resistance at extremely low temperatures. Most of devices developed at SVTA before operate at room temperature or liquid nitrogen temperature, not lower. Our task was to make sure that our contact metallization works well at temperatures close to liquid helium. Since we use n-contacts only, we made several samples with TLM patterns (Fig. 17) of various composition on GaAs, and annealed them in various regimes. Then, wafers have been diced, chips have been packed with wire bonding to each pad, and tested in He cryostat. This experiment demonstrated that our standard technology, which works well down to 77K, gives pronounced diode like I-V characteristics at lower temperatures. The best results we obtained with following contact metallization:

| | |
|---|---|
| Ni | 80 Å |
| Au | 300 Å |
| Ge | 300 Å |
| Au | 300 Å |
| Ag | 1000 Å |
| Au | 3700 Å |

The sample has been annealed at 500°C for 30 seconds. Lower temperature annealing leads to small Shottky barriers at very low temperatures.

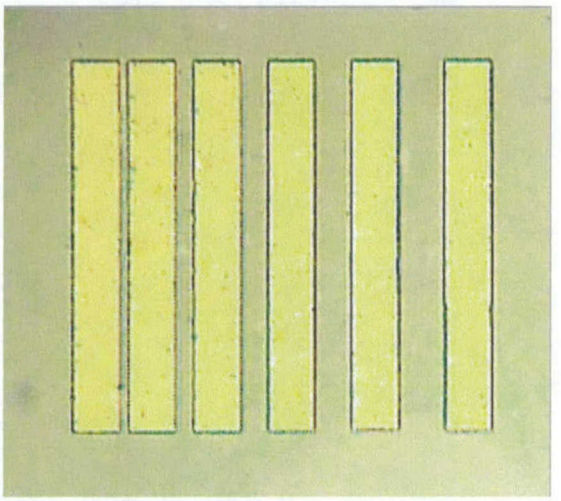

**Fig. 17**. Contact metal TLM pattern on n- GaAs surface.

Ordinary TLM technique but applied at cryogenic temperatures has been used to determine contact resistance per square centimeter. Fig. 18 shows typical plot of resistance as a function of a distance between pads. It allows to conclude that the resistance of a contact pad at 14 K is about 1 Ohm. Our pads were 20 μm x 160 μm

in size. Thus, we have about $3 \cdot 10^{-5}$ $\Omega/cm^2$ serial resistance, which is acceptable level for such low temperature.

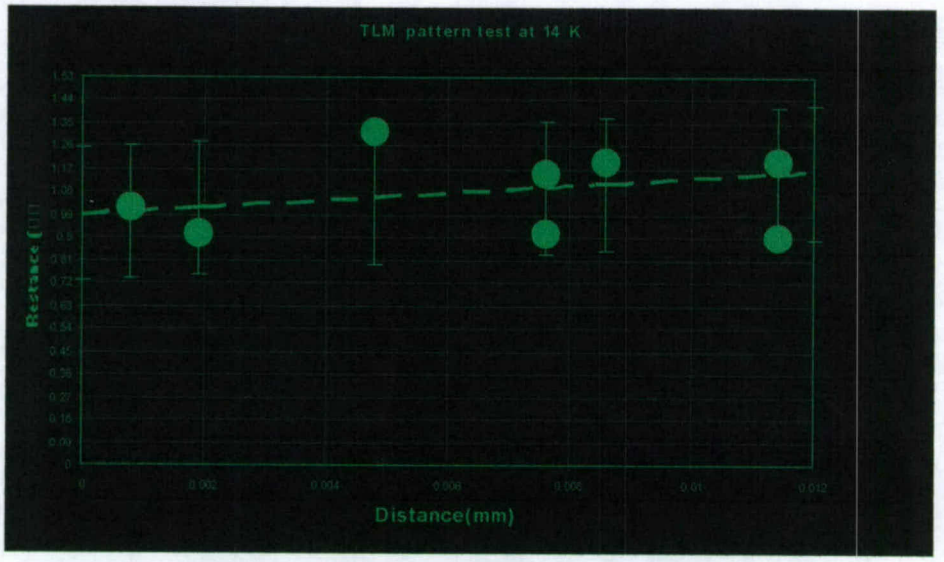


**Fig. 18.** Dependence of the contact resistance on the distance between pads of TLM pattern taken at cryogenic temperatures (14 K).

To provide good heat sinking we used metal-coated CVD diamond heat spreaders from Diamonex. Laser dies were mounted epi-down using soft low temperature soldering alloy. We mounted top contact by metal spring wet with liquid Ga – since it must be placed in deep narrow groove (Fig. 19).

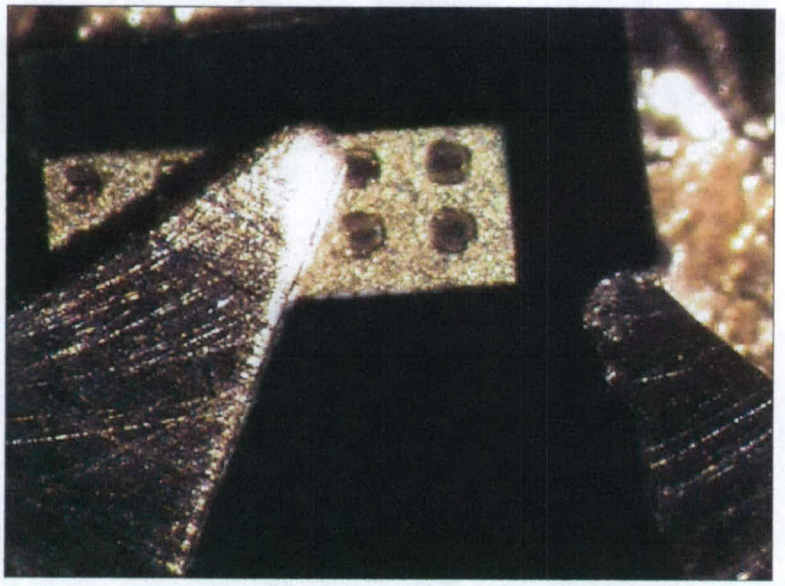

**Fig. 19**. Laser chip with two rows of contact wells on its substrate side is mounted on CVD diamond heat spreader with metal Ga and fixed with spring top contact of the cryostat cold finger.

In this design active layer of the laser is pumped laterally from both sides. Experimental data shows that lateral current spreading in quantum cascade structures may exceed 100 μm, if material quality is good enough. Bottom contact of the laser was connected to the top metallization layer of the diamond heat spreader.

## Testing Methods and Testing Setup

Measurements of terahertz radiation require special technique. Apart from expensive detectors sensitive in this spectral range, there are additional complications caused by asymmetric far field of radiation from such lasers, their low average power in pulsed mode, and geometry of the cryostats used for testing. Most of Ge detectors used for this purpose require very low temperatures close to the liquid He temperature. It has been decided that the most convenient way for preliminary testing of such lasers, used by many groups, is investigation of details of their I-V curves, namely IdV/dI dependence (Fig. 20).

This method is based on fact that at lasing threshold non-equilibrium carrier lifetime in active region of semiconductor laser begins to shrink, and correspondingly, quasi-Fermi levels stabilize. It changes differential resistance of the device. Moreover, lasing can lead to spatial re-distribution of current, causing pronounced kinks in laser I-V curve. Revealing such kinks with real time data processing allows to reliably detect lasing threshold and, in multimode lasers, modal switching points.

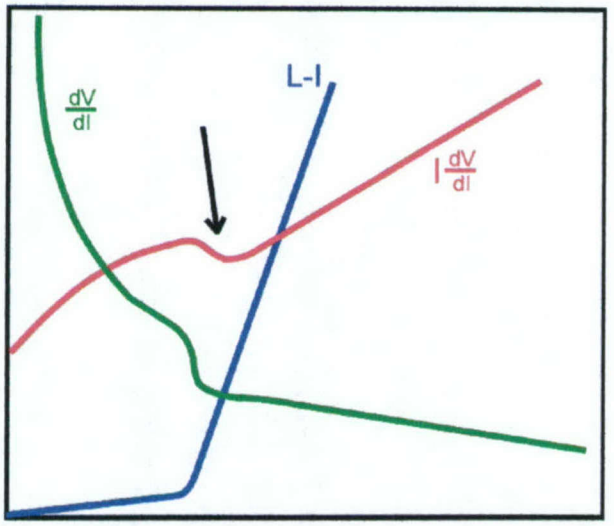


**Figure 20.** Example I dV/dI plot for measuring threshold in a laser diode. Quasi-Fermi levels "freeze" at the threshold, causing peculiarities of I-V dependence. Threshold can be determined from purely electrical data in this manner.

Such method allows to reliably detect lasing threshold. Using this approach makes it possible to study temperature dependence of the threshold current, dependence of the threshold current on cavity length, etc. However, as a difference from standard I

dV/dI measurement which is typically done under DC pumping, we used pulsed excitation, to avoid sample heating. This must allow us to simplify packaging of lasers.

For pulsed I dV/dI tests SVT Associates purchased very sensitive computer based digital oscilloscope (GaGe compuscope). In combination with computer controlled pulsed current source and temperature controlled He cryostat, it will allow us to make I-V measurements with very high resolution in wide range of temperatures. Currently, the system is installed in powerful PC and corresponding software writing is in progress.

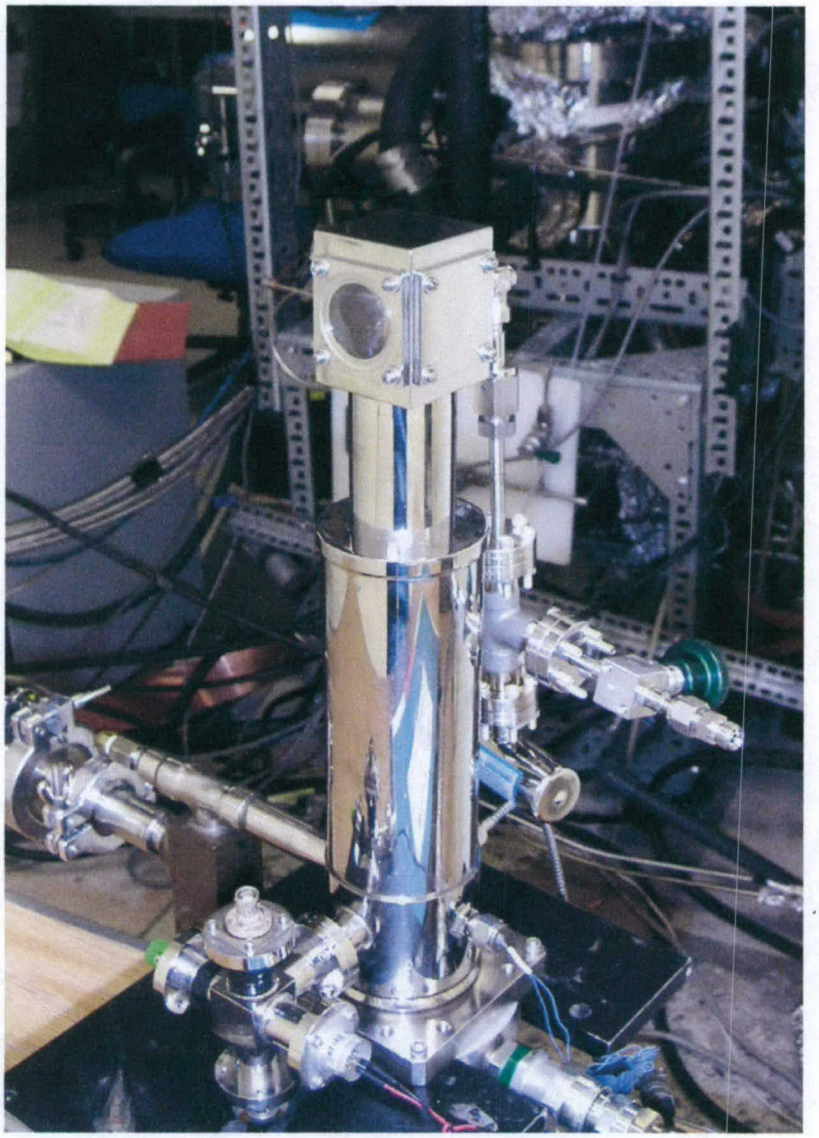

**Fig. 21**. Helium cryostat for THz laser testing

Testing of THz quantum cascade lasers requires very low temperatures. To provide such temperatures, especially for this program we installed a closed cycle helium

cryostat. The cryostat was capable to reach temperatures as low as 15K without any external power applied to the cold finger. However, since we apply significant power to our samples, it has been decided to install additional cold shielding to secure low temperature operation.

Another necessary modification for the cryostat is installation of low impedance ribbon waveguide cable, to deliver pulsed current to the sample without distortion of its shape. This is essential for the pulsed IdV/dI measurements, which we selected as a method of primary lasing test. Existing standard wiring in the cryostat allows only DC current or DC bias. Low impedance ribbon waveguides by ILX Lightwave provide perfect matching with laser diodes and QCLs and can operate at low temperatures.

Pulsed current source which we use is allows resolution as good as 10 μA in pulse amplitude (when under GPIB control). In combination with GaGe compuscope and under special program using LabView interface it allows to study current pulse shape, in particular the decay in applied voltage caused by heating of heterostructure during the current pulse (Fig.22, top indicator).

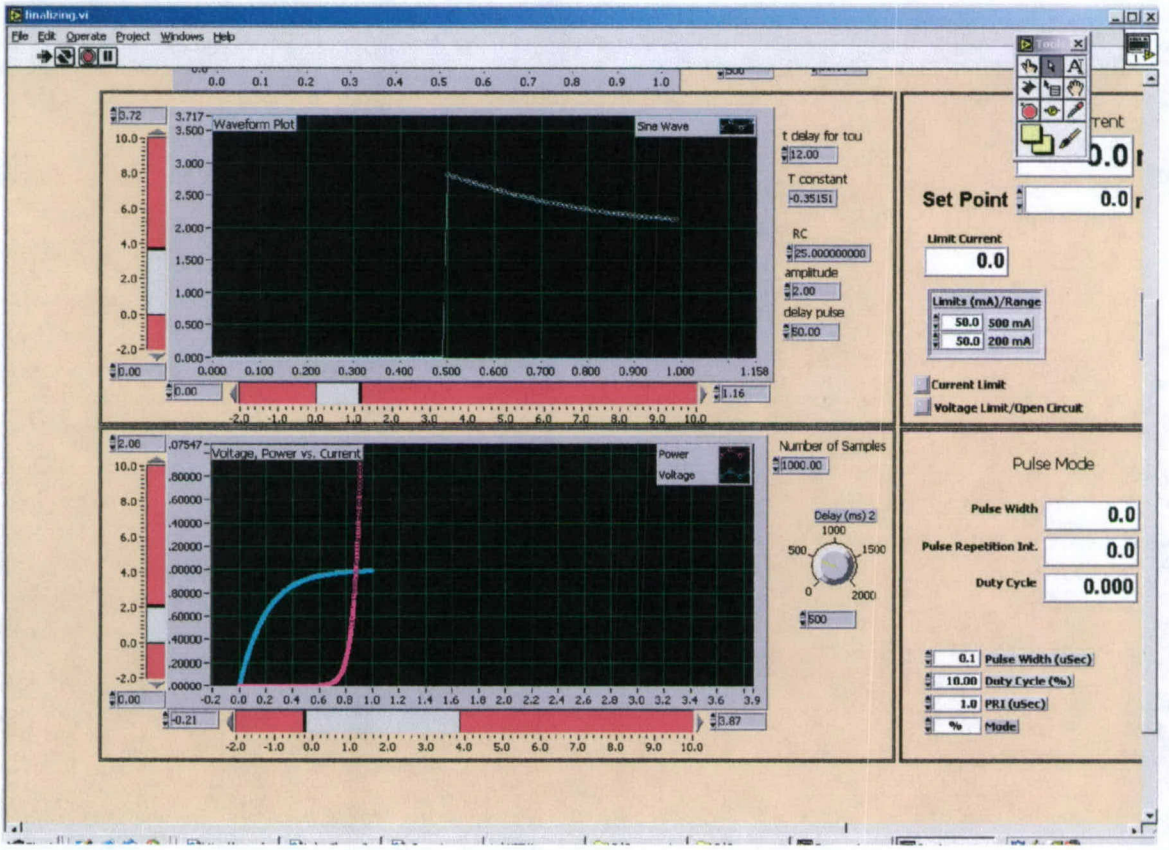


**Fig. 22.** LabView program: Panel 1, Measurements of LIV dependence

This effect, caused by bandgap reduction with increasing temperature may allow us to evaluate real temperature of active region and optimize packaging for minimum thermal resistance. Good time resolution of the GaGe compuscope provides temperature measurements on a scale of microseconds. The system allows measurement and plotting of LIV curves in real time with high resolution by gradual changing the amplitude of the current pulse (Fig. 22, bottom indicator). In addition, the software is designed to control and indicate temperature dynamics of the cold finger during measurements (Fig. 23, top indicator). With all these data acquired, it is possible to calculate pulsed IdV/dI value and plot it in real time (simulated curve is shown in the bottom indicator, Fig. 23).

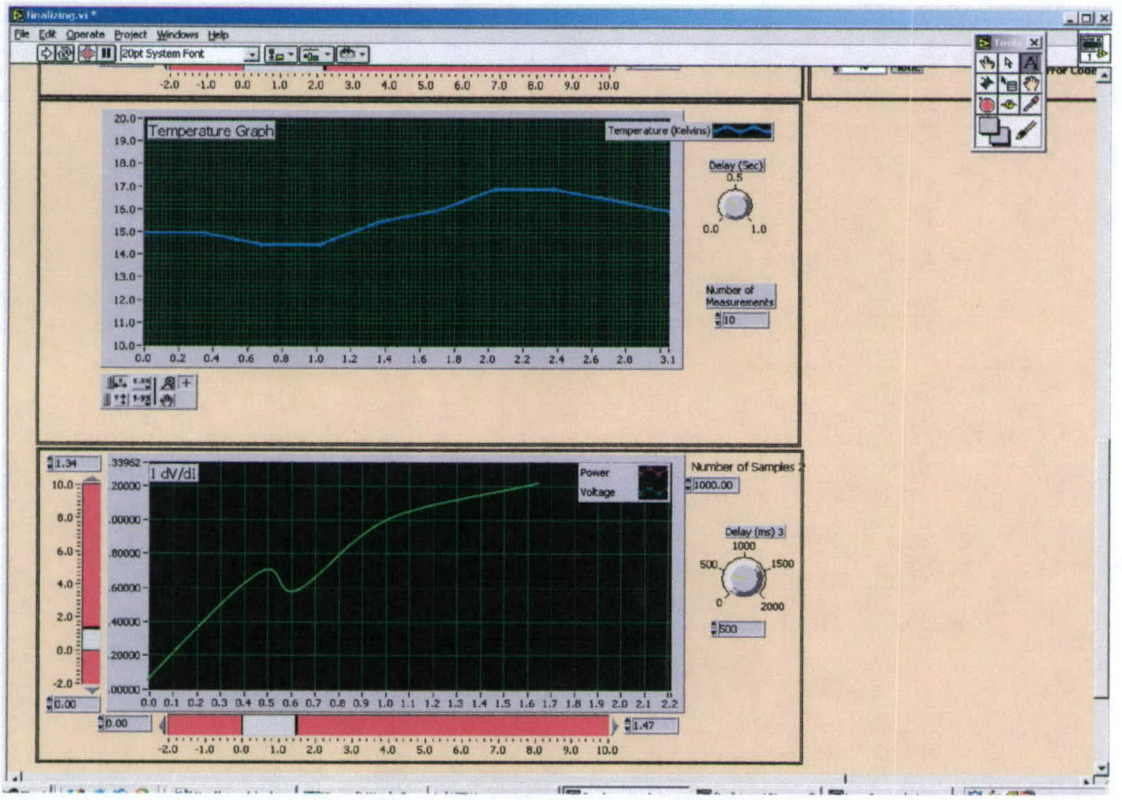


**Fig. 23.** LabView program: Panel 2, Temperature control and IdV/dI indicator

## Testing Results and Analysis

Before THz laser measurements, the IdV/dI testing system has been verified and calibrated with infrared lasers. In this case we were capable to measure their optical output directly as well. We kept duty cycle as low as 1%, and pulse duration as short as 2 μs. This has been done to avoid any significant heating of the active region of the laser. Fig. 24 presents results of testing industrial single mode high efficiency 980 nm laser. This laser demonstrates pronounced kink in its I-V curve at the lasing

threshold. L-I curve shows photodetector saturation due to high output power. Very pronounced kink on the IdV/dI curve exactly coincides with the lasing threshold.

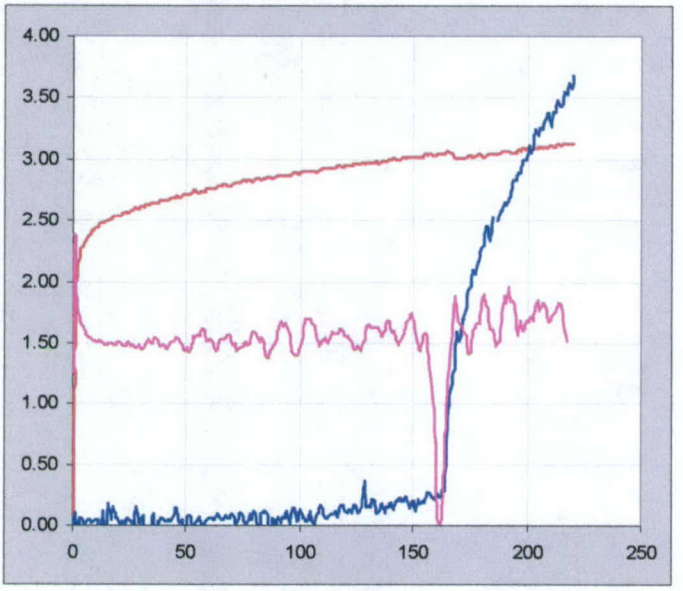


**Fig. 24.** Pulsed IdV/dI testing of industrial high efficiency single mode 980 nm laser: I-V curve (red), L-I curve (blue), IdV/dI curve (pink).

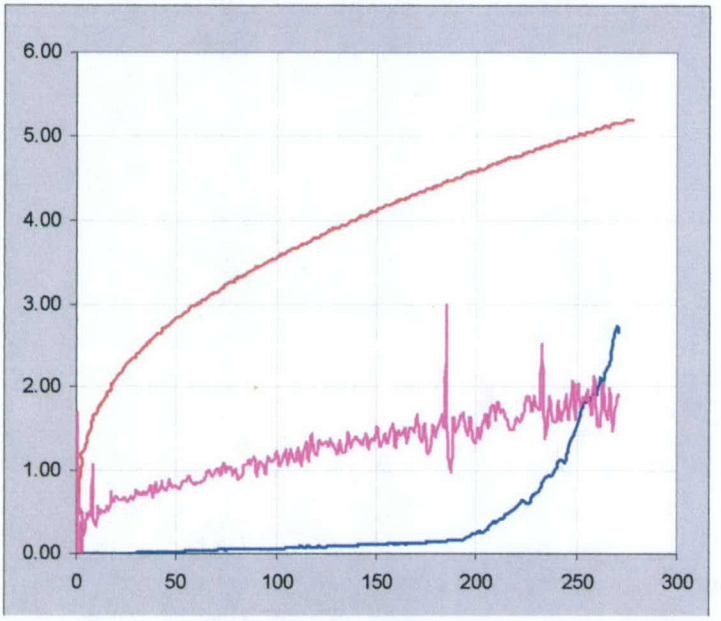


**Fig. 25.** Pulsed IdV/dI testing of multi-mode MIR laser (2.5 μm wavelength): I-V curve (red), L-I curve (blue), IdV/dI curve (pink).

To test the method and setup even more, we studied experimental samples of MIR lasers made by SVTA. These lasers were multimode, and lasing threshold was not so steep and pronounced. Their I-V curves did not demonstrate obvious kink at lasing threshold; however, it still showed up in the IdV/dI plot. Secondary kinks in this curve typically indicate laser switching to higher order mode operation, with corresponding spatial re-distribution of injected carriers (Fig. 25). Such kinks above the lasing threshold were expected in THz lasers, too.

Additional difficulties with THz laser testing comparing with room temperature ones were related to RF noise generated by the operating cryostat. However, installing electrical shields and time averaging allowed us to get clear and distinguished peaks in IdV/dI dependence measured at low temperatures. Fig. 26 demonstrates such IdV/dI response from the sample mounted on diamond heat sink similarly to one shown in Fig. 19. The sample is made out of the "reference" wafer, and we attribute it to the lasing threshold. However, the threshold current density observed in samples made of this wafer, was significantly lower, than one reported in original paper (APL v.81, 8, pp.1382-1383). We believe that this improvement is due to the undoped substrate which we used for the wafer growth, and due to the corresponding changes in laser design leading to significant reduction in optical losses.

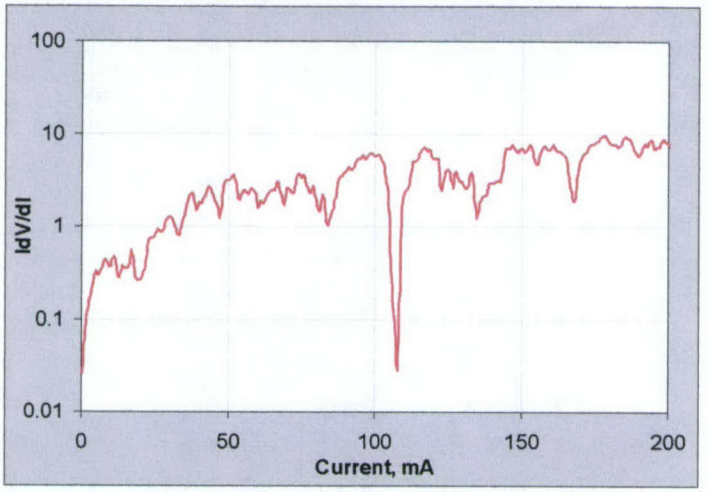


**Fig. 26.** Example of pulsed IdV/dI curve of "classical" THz QC laser for 66 μm radiation at 35K. Pronounced kink at 110 mA we attribute to lasing threshold.

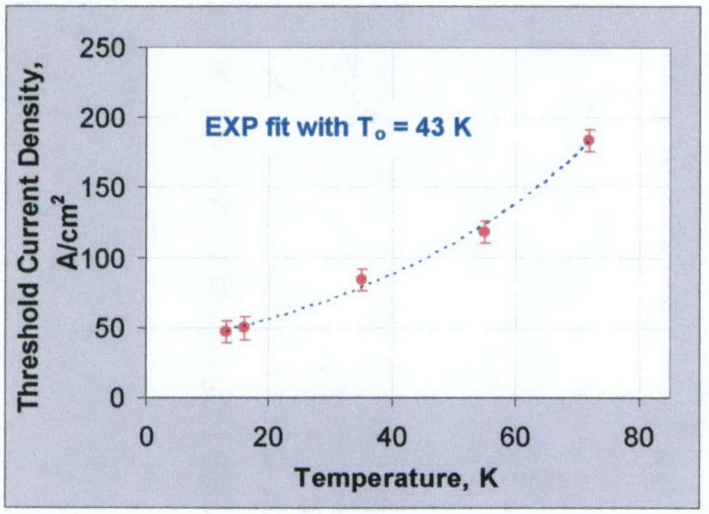


**Fig. 27.** Temperature dependence of the lasing threshold in "reference" structure laser. Its pronounced exponential increase with temperature is illustrated by fit having characteristic temperature $T_0 = 43$ K (blue dashed line).

Temperature dependence of the threshold current detected by this method is shown in Fig. 27. It increases exponentially with temperature, which is in good agreement with typical laser behavior. Characteristic temperature of this dependence $T_o$ is approximately 43 K. It is important to notice, that significant reduction of the threshold current density (4 times, from 210 A/cm$^2$ down to 50 A/cm$^2$) allowed our lasers to operate almost up to liquid nitrogen temperature. In addition, our device had no high reflecting coating on its back facet, and was significantly shorter than the laser reported in the reference. With this option, we believe, lasers having our novel geometry may operate even at liquid nitrogen temperature.

Lasers with three different stripe width have been manufactured and tested. Lasing has been demonstrated in devices with 100 μm and 75 μm wide stripes. Latest devices demonstrated significantly higher thresholds. None of the devices with 50 μm stripe width demonstrated any kinks in IdV/dI dependence which could be interpreted as lasing threshold. This effect may be partly due to the problem of undercut while making back contact wells. The ridge between wells in 50 μm lasers was significantly narrower than in 100 μm or 75 μm ones, and may not serve as good waveguide.

**Coupled Quantum Wells Quantum Cascade Terahertz Lasers for 30 μm Radiation**

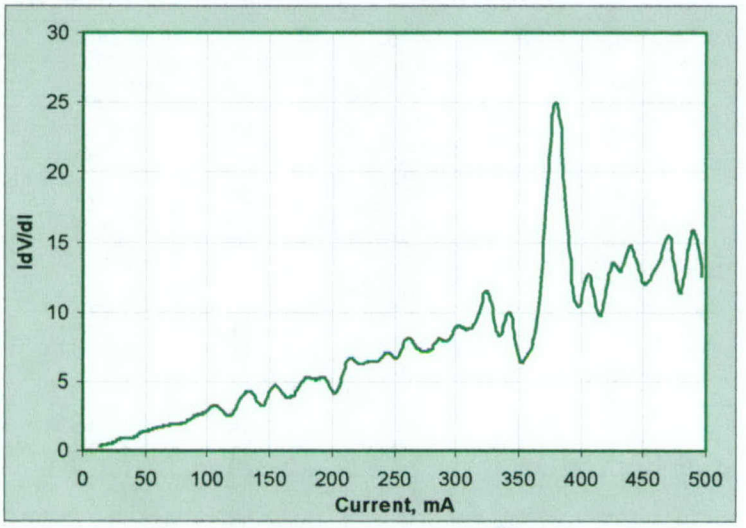


**Fig. 28.** Example of pulsed IdV/dI curve of THz "coupled quantum wells" structure laser designed specially for this project. Measurement has been done at 18 K. Pronounced kink at approximately 380 mA we attribute to lasing threshold.

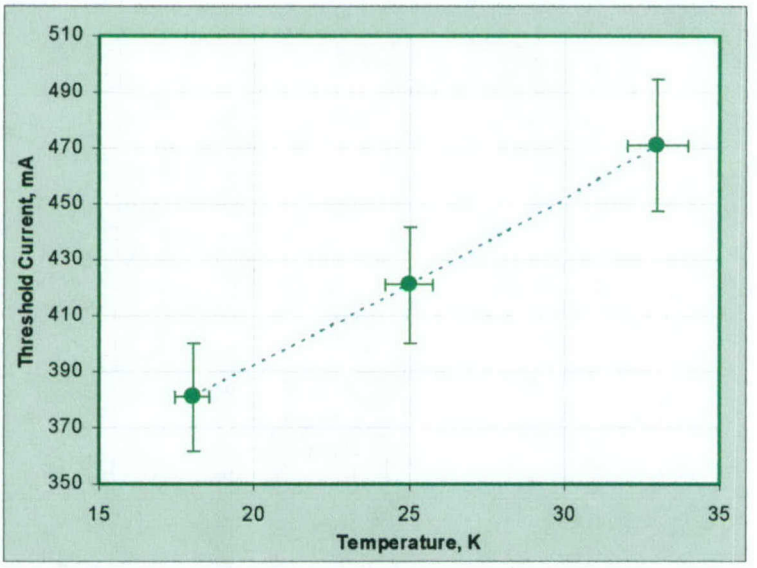


**Fig. 29.** Temperature dependence of the lasing threshold in "coupled quantum wells" structure laser designed for this project. Exponential fit having characteristic temperature $T_0 = 71$ K is shown in dashed line.

Lasers with novel design (based on coupled quantum wells) were manufactured and tested in similar way. Fig. 28 demonstrates one of the IdV/dI curves obtained from this structure. Lasing occurs at approximately 380 mA, which is 5 times more than lasing threshold in "reference" structure. However, this laser is designed for 30 μm

wavelength (as a difference from "reference" laser, designed for 66 mm radiation), and employs novel principle. Further optimization of this very first structure based on "coupled quantum wells" principle may allow reducing threshold currents.

In existing lasers with such design of the active region, significant heating of the active region takes place even under 1% duty cycle pulsed mode excitation with pulse duration as short as 2 μsec. This did not allow us to test lasers below 18 K. When increasing the temperature, we observed lasing up to 33 K only. This data, presented in Fig. 29, allows us to evaluate characteristic temperature of such lasers to be approximately 70 K.

## Conclusions

- It has been demonstrated that our technology allows us to grow 3" terahertz quantum cascade structure wafers with quality necessary for their successful operation.

- Novel design of THz QC laser structure for emission at 30 μm wavelength based on coupled quantum wells has been developed and corresponding wafers have been grown. It have been demonstrated to have lasing operation with $T_0$=70K up to 33K temperature.

- A separate electric and waveguiding (SEW) laser geometry has been tested which permits using undoped substrates to significantly reduce optical losses in laser cavity, resulting in higher operating temperature and lower lasing threshold. Threshold current density as low as 50 A/cm$^2$ has been obtained in "reference" 66 μm structures due to novel device geometry. This is 4 times lower than reported in similar structures with doped substrate.

- Lasing in 66 μm THz laser structures has been demonstrated at temperatures up to 72 K, which is close to liquid nitrogen temperature and is almost 30 degrees higher than in similar structures with doped substrate. Characteristic temperature of 43 K has been demonstrated in 66 μm structure "classical wafer design" SEW lasers.

## Future Development Plan

Results obtained during this Phase I work suggest direct power measurements of the laser output beam, which can be done using custom made germanium detector operating at liquid helium temperature. We plan to perform such test in near future in collaboration with University of Central Florida. We will setup special liquid helium cryostat with dual temperature control for this task: one for the detector and one for the THz laser.

Another task is to achieve lasing at liquid nitrogen temperature. This task may not require new wafer design or growth. We hope to solve it by cavity optimization, i.e. selection of optimum cavity length and stripe width, and, possibly, by deposition of high reflective coating on the rear facet of the laser. This coating at current stage may be simple, consisting of dielectric and metal layers.

More significant improvement of the THz laser can be accomplished in Phase II project. In particular, further improvement of the laser waveguide will be accomplished. Currently, all THz QC lasers have strongly asymmetric waveguides, where active layer is located in the very edge, close to the wafer surface. This greatly reduces confinement factor of radiation in active region, and thus increases laser threshold and reduces its power efficiency. Such situation is caused by problems with MBE growth of layers having thickness, comparable with the wavelength of THz radiation, to form symmetric waveguide. Ideally, active region should be located in the center of a waveguide having thickness, comparable with radiation wavelength in semiconductor material.

We propose a new concept to overcome this bottleneck. SVTA has unique combination of expertise in MBE growth and wafer bonding. Currently, we evaluate consider possibility of bonding together two AlGaAs THz QCl wafers, so that after lapping they may form a symmetric waveguide having total thickness comparable with the wavelength of the laser radiation in semiconductor. We expect not only significantly reduced threshold and improved efficiency in such laser, but also much better output beam properties. Currently, the output beam of existing QC THz lasers is asymmetric, and most of the energy goes downwards the substrate, making it difficult to utilize it. By improving the waveguide, we may increase the percent if output power which can be utilized by systems, employing such lasers.

In this case we again should use undoped substrates to reduce optical losses due to free carrier absorption. To deliver current to the active region, we can apply same novel SVTA approach which we successfully demonstrated in Phase I work, namely lateral pumping through deep wells. However, such lasers will require additional work on advanced packaging to provide improved thermal management. We plan numerical simulations to develop corresponding packaging. These concepts are illustrated in the figure below.

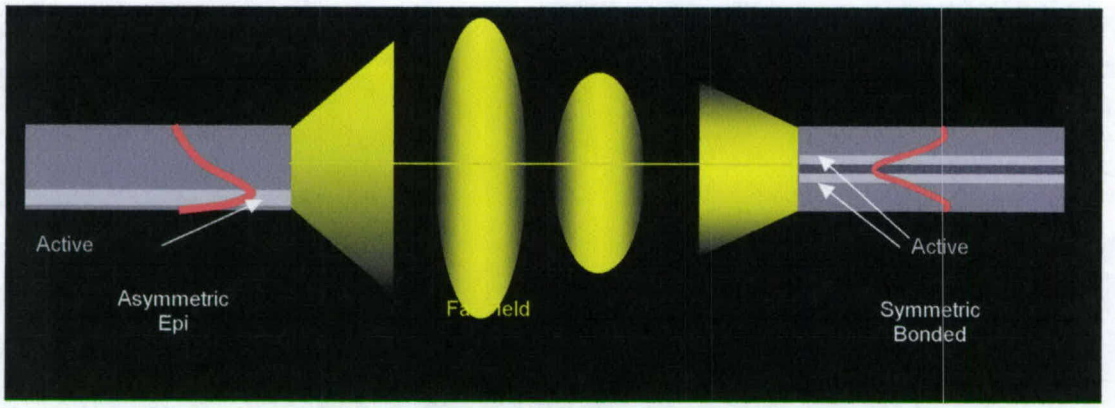


Expected mode profile and far field pattern in ordinary and bonded SEW THz lasers.